J Mater Sci: Mater Electron (2014) 25:730–735
DOI 10.1007/s10854-013-1637-9

A novel microwave synthesis of nanocrystalline SnO_2 and its structural optical and dielectric properties

M. Parthibavarman · K. Vallalperuman · S. Sathishkumar · M. Durairaj · K. Thavamani

Received: 27 September 2013 / Accepted: 23 November 2013 / Published online: 1 December 2013

Abstract Nanocrystalline SnO_2 particles with the rutile structure have been successfully synthesized by a novel microwave irradiation method. This process requires less reaction time and low temperature. Transmission electron microscopy studies show that SnO_2 particles are in spherical shape with size about 25–30 nm. Selected area electron diffraction pattern confirms single crystalline nature of the SnO_2. UV–Vis spectrometer was carried out to study the optical properties and estimated band gap energy of SnO_2 particles is 3.55 eV. In Fourier transform infrared study, a defined peak at around 615 cm^{-1} is observed due to Sn–O vibration. Frequency dependent dielectric anomaly is observed in SnO_2 nanoparticles at low temperature. It is found that the value of dielectric constant of SnO_2 particles at 10 kHz is found to be 777.5. It systematically decreases with increasing frequency whereas increases with increasing temperature. Further, the prepared samples were characterized by Photoluminescence spectroscopy and energy dispersive spectroscopy.

1 Introduction

In recent years, metal oxide based semiconducting nanostructures have rapidly become one of the fastest growing fields in the materials chemistry and physics [1]. Transition—metal oxide nanomaterials such as SnO_2, ZnO, TiO_2 and WO_3 have attracted a great deal of interest due to their unique physical and chemical properties. As a result, it could find potential applications in next-generation electronic and optoelectronic devices. In metal oxide semiconductors (such as SnO_2, ZnO, WO_3, TiO_2 etc.), electrical conductivity strongly depends on the composition of a gas and its surrounding area. Therefore they are very popular and useful sensing materials for making inexpensive gas sensing devices [2]. Among various kinds of metal oxide semiconductors, SnO_2 semiconductors have been keenly studied due to their excellent chemical stability and optical and electrical properties [3].

SnO_2 particles are an n-type semiconductors with a wide band gap ($E_g = 3.6$ eV, at 27 °C) and which are well known for various potential applications such as excellent gas sensors, electrode materials in Li/SnO_2 batteries, catalysts [4] and so on. Many methods have been adapted to synthesis SnO_2 nanoparticles such as, chemical precipitation [5], sol–gel [6], hydrothermal [7], solvothermal [8], spray pyrolysis [9] and thermal evaporation [10]. Compared with the above processes, the microwave method has sparked much interest due to their operation simplicity, effective, low-cost route to synthesis, less time consuming (about 10 min), and for large-scale production. In this work, the authors have prepared tin dioxide nanoparticles in short time (10 min) by using reducing agent without any post-synthesis modifications. Hydrazine hydrate is a convenient reluctant, since the by-products are typically nitrogen gas and water [4]. Hydrazine hydrate was added (drop by drop) into the precursor solution, with stirring, until the light grey precipitates were obtained. Hydrazine hydrate absorbs more microwave energy than ammonia which results in increased reaction rate. To best of our knowledge, this is the first preliminary report about

M. Parthibavarman (✉) · K. Vallalperuman · S. Sathishkumar · M. Durairaj
Department of Physics, Mahendra Engineering College, Tiruchengode 637 503, Tamilnadu, India
e-mail: varmanphysics85@gmail.com

K. Thavamani
Department of Physics, AVS Technical Campus, Salem 636 106, Tamilnadu, India

structural, optical and gas dielectric properties of SnO_2 nanoparticles prepared by simple and less time consuming microwave irradiation method.

2 Experimental procedure

In a typical experimental procedure, $SnCl_2{\cdot}2H_2O$ (analytical grade) was dissolved in deionized water to make 0.1 M solution. The hydrazine hydrate solution was added drop wise under strong stirring until the pH of the solution reaches to 7. When the reaction is complete, an azury precipitate was obtained. This precipitate was washed with water more than ten times until no chlorine ions are detected in silver nitrate test. The resulting precipitate was transferred into teflon lined household microwave oven (2.45 GHz) with power up to 900 W and irradiated for 10 min. Finally light grey colored precipitate was dried at 70 °C.

2.1 Characterization

The structure and crystallite size was analyzed by powder X-ray diffraction (XRD) using Bruker diffractometer within the 2θ range of 10°–80° using CuKα as X-ray source (λ = 1.5406 Å). The particle size and morphology were analyzed using transmission electron microscopy (TEM) and selected-area electron diffraction (SAED) pattern was recorded on a Technai G20-stwin high resolution electron microscope (HRTEM) using an accelerating voltage of 200 kV. Optical properties were analyzed by UV–Vis diffusion reflectance spectroscopy using CARY 5E UV–Vis–NIR spectrometer in the wavelength range of 200–800 nm. Photoluminescence spectra of the samples were collected at room temperature by using Cary Eclipse (el02045776) Fluorescence spectrophotometer in the wavelength range of 400–800 nm with a Xe laser as an exciting source, and excitation wavelength of 350. The Fourier transformed infrared spectra (FT-IR) of the samples were collected using a 5DX FTIR spectrometer. SnO_2 powder is pressed into pellet form by using hydraulic pelletizer. Dielectric measurements at low temperature are performed by HP 4192A LF Impedance Analyzer (5 Hz–13 MHz) with fully automated dielectric measurement set up.

The overall reactions in the microwave process are presented in the form of equations

$$3N_2H_4 + 4H_2O \rightarrow 4NH_4OH + N_2 \quad (1)$$

$$Sn^{4+} + 4NH_4OH \rightarrow SnO_2 \downarrow + 4NH_4^+ + 2H_2O \quad (2)$$

As represented in reaction (1), OH^- ions were formed via the dissociation of N_2H_4 into NH_4OH and N_2 [9].

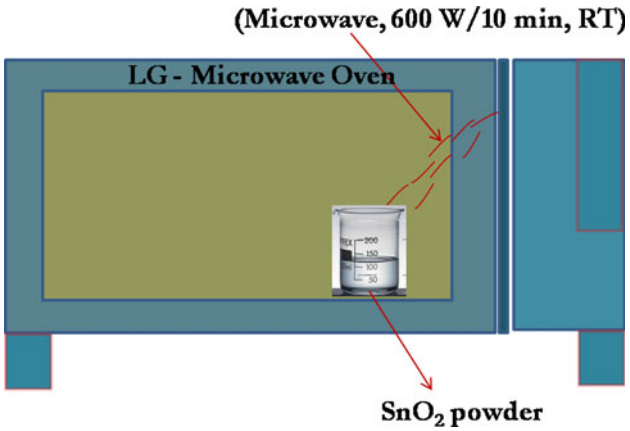

Fig. 1 Schematic illustration for synthesis of SnO_2 nanoparticles in microwave atmosphere

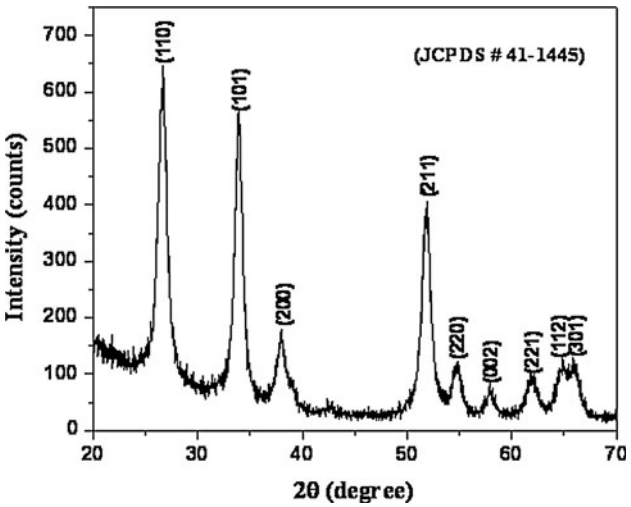

Fig. 2 XRD pattern of SnO_2 nanoparticles

Reaction (2) represents the formation of the SnO_2 nanoparticles via the reaction between Sn^{4+} and OH^- ions formed in reaction (1). Figure 1 shows the schematic illustration of synthesis of SnO_2 nanoparticles under microwave atmosphere.

3 Results and discussion

3.1 XRD analysis

The phase formation and purity of the as-synthesized SnO_2 nanoparticles were investigated by XRD as shown in Fig. 2. All the diffractions peaks can be perfectly indexed to the tetragonal SnO_2 rutile type structure. The following miller indices [110], [101], [200], [211], [220], [002], [221], [112] with calculated lattice parameters of a = 0.481 nm and c = 0.322 nm, are in good agreement with the standard

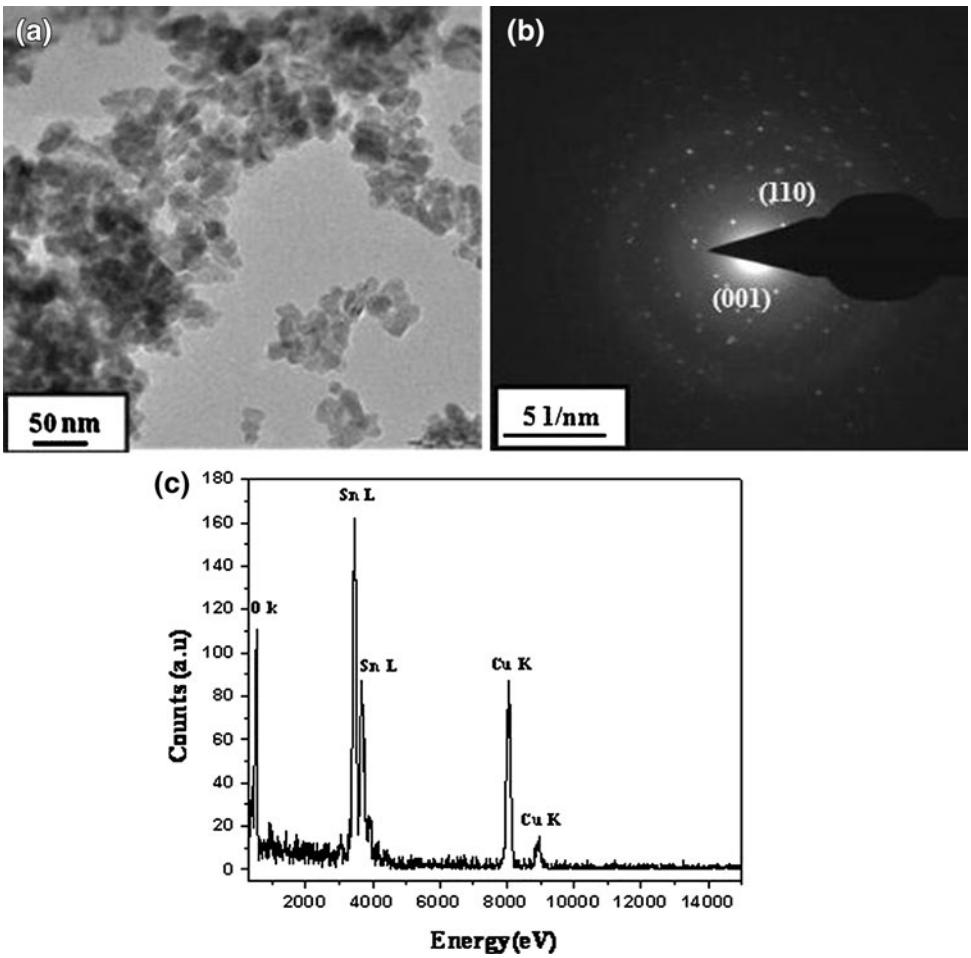

Fig. 3 **a** TEM image of SnO_2, **b** corresponding SAED pattern, **c** energy dispersive spectroscopy

JCPDS (# 41-1445) data. The average crystalline size of the nanoparticles were calculated by using Scherrer's equation

$$d = \frac{K\lambda}{\beta \cos\theta}$$

where d is the mean crystalline size, K is the constant taken as 0.89, λ is the wavelength of the incident beam, β is the full width at half maximum. The average crystalline size of SnO_2 was found to be 30 nm.

3.2 TEM analysis

The morphology and particle size of the tin dioxide nanoparticles were analyzed using TEM micrograph (Fig. 3). Figure 3a shows TEM image of SnO_2 nanoparticles. It clear from the figure that spherical shaped nanoparticles have been formed. The average particle size is estimated to be 25–30 nm. Thus calculated particle sizes are in very good agreement to those calculated from XRD data. Figure 3b shows the corresponding SAED pattern and it showed bright and sharp spots, which have been indexed to the tetragonal rutile phase with single crystalline nature. The calculated particles size from XRD investigation matches well with the particles size observed from TEM micrograph. These results reveal the formation of single crystalline nature of the sample. TEM based energy dispersive spectroscopy (EDS) analysis is shown if Fig. 3c. It confirms that the nanoparticles mainly consist of Sn and O element, and average Sn/O atomic ratio is 1:1.95, which exhibits the O-deficient condition of the nanoparticles. The Cu element was found in the composition, due to the grid used to for EDS measurements.

3.3 UV–Vis diffusion reflectance spectroscopy

The optical properties were analyzed using UV–Vis diffusion reflectance spectroscopy. Figure 4a shows the UV–Vis diffusion reflectance spectra of SnO_2 nanoparticles. The diffusion reflectance, R of the sample is related to the Kubelka–Munk function F(R) by the relation

$$F(R_\infty) = (1 - R_\infty)^2 / 2R_\infty = k/s = Ac/s$$

F(R∞) is the so called remission or Kubelka–Munk function, where k is the absorption coefficient, s is the

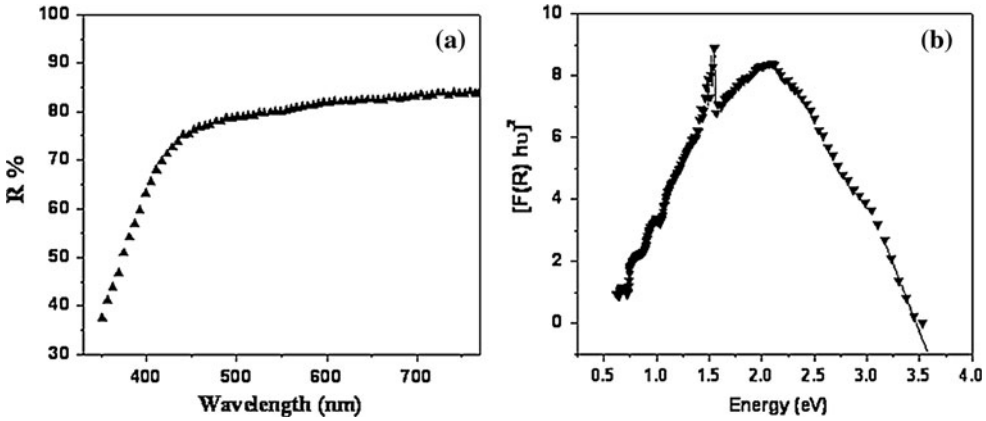

Fig. 4 **a** UV–Vis DRS spectra of SnO_2, **b** corresponding Kubelka–Munk model

scattering coefficient, c is the concentration of the absorbing species, A is the absorbance and R is the reflectance [11]. The spectra used for the band gap calculations are plotted in terms of F(R). The band gap energy of SnO_2 nanoparticles were calculated from their diffusion reflectance spectra by plotting the square of the Kubelka–Munk function $F(R)^2$ versus energy in electron in volts. The linear part of the curve was extrapolated to $F(R)^2 = 0$ to get the direct band gap energy (see in Fig. 4b). Estimated band gap energy of SnO_2 particles is found to be 3.55 eV. This value is in good agreement with the reported value [2].

3.4 Photoluminescence spectroscopy

Photoluminescence spectrum is convenient to investigate the structure and defect or impurity levels. Figure 5 shows the room temperature PL spectrum of SnO_2 nanoparticles. The excitation wavelength used for the PL measurements is 350 nm (3.54 eV), with a Xe laser as an exciting source. The PL spectrum shows a strong UV emission peak at 371 nm (3.2 eV) and a broad blue emission close to 465 nm (2.5 eV). Since the excitation and emission values are both lower than the band gap of SnO_2 ($E_g = 3.55$ eV), the emission cannot be assigned to the direct recombination of a conduction electron in the Sn 4*p* band and a hole in the O 2*p* valance band. This similar finding was observed by the author Gu et al. [12]. The UV emission is widely reported in the literatures [13] in the present work, UV emission is mainly owing to oxygen vacancies, tin interstitials or dangling bond and structural defects. The broad blue emission to electron transition is mediated by defect levels in the band gap such as oxygen vacancies and tin interstitials [14]. Jin et al. [15] reported that the PL peak at 3.1 eV was due to the structural defects and that of peak at 2.4 eV was related to oxygen vacancies. Therefore, it is complicated to trace the origin of UV and blue emission. For these reasons, the synthesized SnO_2 nanoparticles may

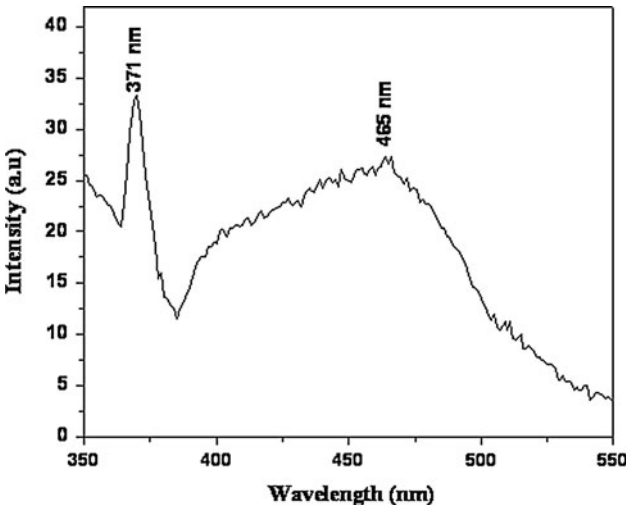

Fig. 5 Photoluminescence spectra of SnO_2 nanoparticles

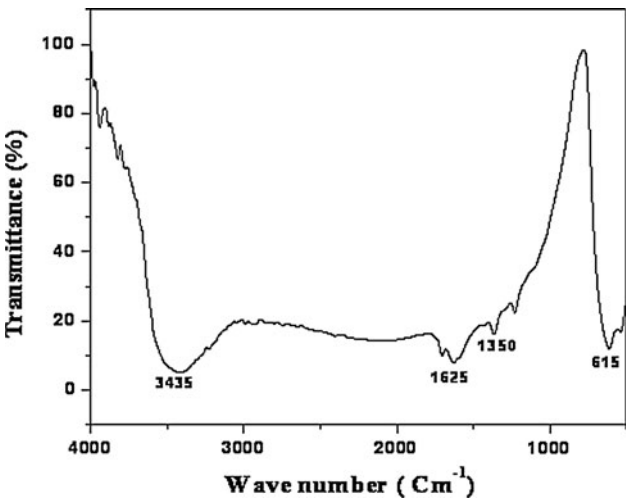

Fig. 6 FTIR spectra of SnO_2 nanoparticles

have large number of defects such as oxygen vacancy, vacancy cluster and lattice disorder at the interface and interior surface.

3.5 FTIR spectroscopy

Figure 6 shows the FTIR spectra of SnO_2 nanoparticles. The absorption bands at 3,435 and 1,625 cm^{-1} attributed to stretching vibration of surface hydroxyl group or adsorbed water. It has been found due to re adsorption of water molecules from ambient atmosphere [16]. The bands observed at 1,350 cm^{-1} in the IR spectra are assigned to a hydroxyl bending mode of different types of surface hydroxyl groups [17]. The peak around at 615 cm^{-1} is observed due to Sn–O vibration [4].

3.6 Dielectric measurement

The dielectric measurement of SnO_2 nanopowders was carried out by using a dielectric cell and an impedance analyzer (model: HP 4192A). Disc shaped samples with 8 mm in diameter is used to find out the dielectric constant. The capacitance and dielectric loss of the sample was measured at various frequencies ranging from 10 kHz–1 MHz. Dielectric constant or relative permittivity was calculated using the relation $\varepsilon_r = Cd/\varepsilon_o A$ and tan $\delta = D\varepsilon$, where, *d* is the thickness of the sample, *C is* the capacitance and *A is* the area of cross section of the sample, ε_r is the relative permittivity of the material and ε_0 is the dielectric permittivity of vacuum (8.854×10^{-12} F/m).

Figure 7 shows the variation of dielectric constant and loss with frequency at temperature 300 K. The dielectric constant rapidly decreases with increasing frequency up to around 90 kHz and thereafter it shows frequency independent behavior. But after 90 kHz it remains almost constant. The variation of dielectric loss with frequency shows dielectric loss decreases exponentially up to 10 kHz. It is well known that dielectric behavior of nanomaterials could be enhanced due to the contribution of two dielectric polarization mechanism such as rotation direction polarization (RDP) process and space charge polarization (SCP) process. It is proposed that both RDP and SCP process contribute more to the enhancement of dielectric response of the SnO_2 nanoparticles [18]. Figure 8 shows the temperature and frequency dependent of dielectric constant (ε_r) of SnO_2 nanoparticles. It reveals that the dielectric constant (ε_r) remains constant up to temperature 250 K, but it increases with temperature after 250 K. The dielectric constant (ε_r) increases with increasing temperature. The maximum values of dielectric constant decrease with increasing frequency. Figure 9 shows the temperature and frequency dependent of dielectric loss of SnO_2 nanoparticles. It is observed that the loss tangent increases as the frequency increases. The a.c. conductivity of SnO_2 (σ_{ac}) calculated with data

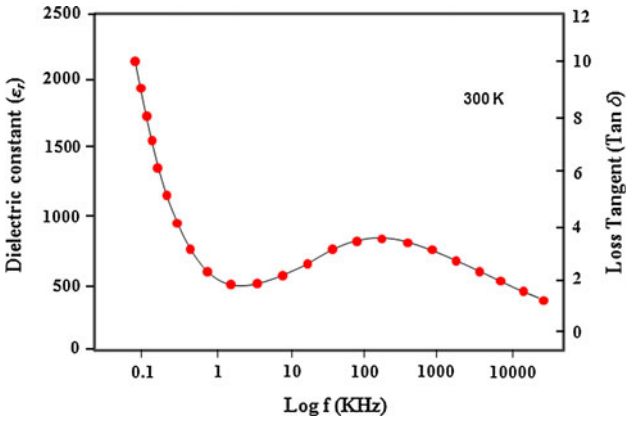

Fig. 7 Dielectric variations of SnO_2 nanoparticles with different frequency at 300 K

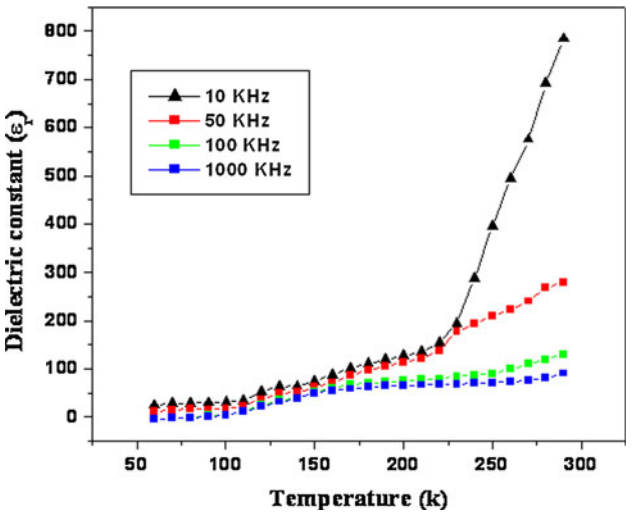

Fig. 8 Variations of dielectric constant with temperature at different frequencies for SnO_2 nanoparticles

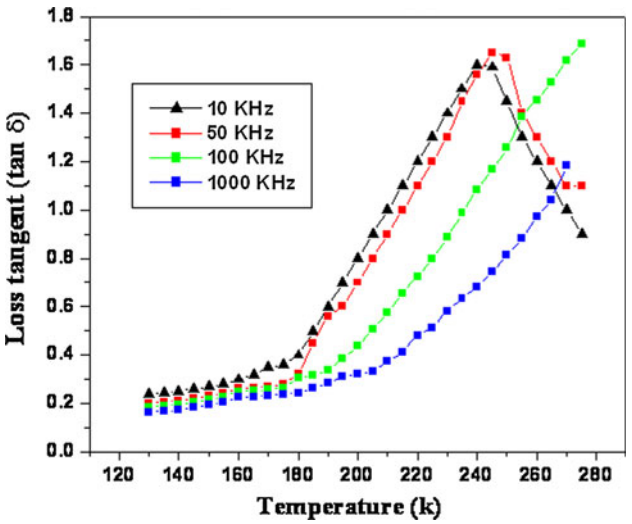

Fig. 9 Change in dielectric loss with temperature at different frequencies for SnO_2 nanoparticles

Table 1 The dielectric constant $(\varepsilon_r)_{and}$ a.c. conductivity (σac) values of SnO_2 at various frequencies

Frequency (kHz)	Dielectric constant (ε_r)	a.c. conductivity (σ_{ac}) 10^{-5} S/m
10	777.5	0.041
50	230.8	0.091
100	98.6	0.15
1,000	34.5	0.21

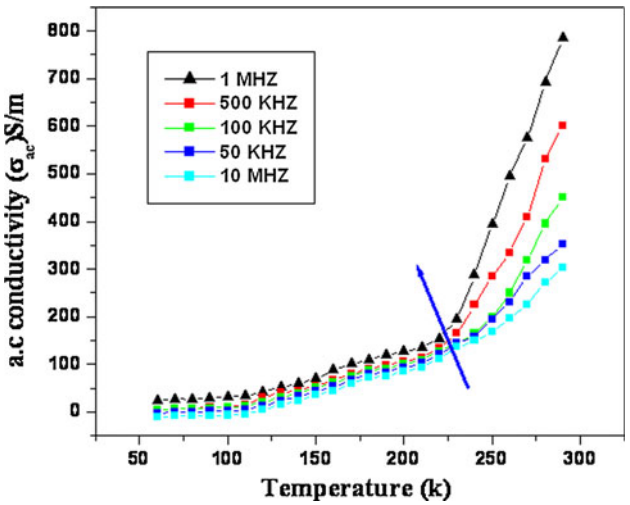

Fig. 10 Change in a.c. conductivity with temperature in SnO_2 nanoparticles

available from the dielectric measurement by using the relation:

$$\sigma_{ac} = 2\pi f \tan\delta\epsilon_0\epsilon_r$$

where, f is the frequency of applied field, tan δ is loss tangent available from dielectric measurement, ε_r is the relative permittivity of the sample and ε_0 is the dielectric permittivity of vacuum (8.854×10^{-12} F/m). Table 1 shows the maximum values of ε_r and σ_{ac} at 300 K for SnO_2 particles at various frequencies. The temperature and frequency dependent of a.c. conductivity is shown in Fig. 10. It is found that a.c. conductivity increase with increase of temperature due to mobility of charge carriers for hopping. Mobility of hopping ions increases with temperature and thereby increasing conductivity. Further, the a.c. conductivity increases with frequency. The involved electrons in hopping are responsible for electronic polarization in SnO_2 [19].

4 Conclusion

SnO_2 nanocrystalline powders were successfully synthesized by a novel microwave irradiation method with in short time. Powder XRD results confirm the tetragonal rutile structure. TEM results indicate that very narrow distribution of spherically shaped nanoparticles (about 25–30 nm) can be achieved by using microwave irradiation method. SAED pattern confirms the single crystalline nature of the sample. The optical band gap energy found to be 3.55 eV. Frequency dependent dielectric anomaly is observed in SnO_2 nanoparticles at low temperature. At low temperature, dielectric constant and dielectric loss decreases with frequency where as it increases with temperature. The increase in a.c. conductivity with temperature is owing to mobility of charge carriers. This is responsible for hopping. Therefore, it is concluded that the prepared microwave assisted SnO_2 nanoparticles could be a potential candidate for high density energy storage materials.

References

1. V. Hariharan, S. Radhakrishnan, M. Parthibavarman, R. Dhilipkumar, C. Sekar, Talanta **85**, 2166 (2011)
2. M. Parthibavarman, V. Hariharan, C. Sekar, Mater. Sci. Eng. C **31**, 840 (2011)
3. M. Parthibavarman, V. Hariharan, C. Sekar, V.N. Singh, J. Optoelect, Adv. Mater. **12**, 1894 (2010)
4. T. Krishnakumar, R. Jayaprakash, M. Parthibavarman, A.R. Phani, V.N. Singh, B.R. Metha, Mater. Lett. **63**, 896 (2009)
5. H. Yang, X. Song, X. Zhang, W. Ao, G. Qiu, Mater. Lett. **57**, 3124 (2003)
6. F. Pourfayaz, A. Khodadadi, Y. Mortazavi, S.S. Mohajerzadeh, Sens. Actuators B **108**, 172 (2005)
7. F. Du, Z. Guo, G. Li, Mater. Lett. **59**, 2563 (2005)
8. C. Fan, X. Song, Z. Yin, H. Yu, S. Sun, J. Mater. Sci. **41**, 5696 (2006)
9. H. Zhu, D. Yang, G. Yu, H. Zhang, K. Yao, Nanotechnology **17**, 2386 (2006)
10. J.Q. Hu, X.L. Ma, N.G. Shang, Z.Y. Xie, N.B. Wong, C.S. Lee, S.T. Lee, J. Phys. Chem. B **106**, 3823 (2002)
11. V. Hariharan, M. Parthibavarman, C. Sekar, J. Alloy. Compd. **509**, 4788 (2011)
12. F. Gu, S.F. Wang, C.F. Song, M.K. Lu, Y.X. Qi, G.J. Zhou, D. Xu, D.R. Yuan, Chem. Phys. Lett. **372**, 451 (2003)
13. T.W. Kim, D.U. Lee, Y.S. Yoon, J. Appl. Phys. **88**, 3759 (2000)
14. L.M. Fang, X.T. Zu, Z.J. Li, S. Zhu, C.M. Liu, L.M. Wang, F. Gao, J. Mater. Sci. Mater. Electron. **19**, 868 (2008)
15. J. Jin, P.C. Seong, I.C. Cha, C.S. Dong, S.P. Jin, Solid State Commun. **127**, 595 (2003)
16. T. Krishnakumar, N. Pinna, K. Prasanna Kumari, K. Perumal, R. Jayaprakash, Mater. Lett. **62**, 3437 (2008)
17. J. Zhu, Z. Lu, S.T. Aruna, D. Aurbach, A. Gedanken, Chem. Mater. **12**, 2557 (2000)
18. P. Boguslawski, E.L. Briggs, J. Bernholc, J. Phys. Rev. B **51**, 17255 (1995)
19. M. Ghosh, C.N.R. Rao, Chem. Phys. Lett. **393**, 493 (2004)